

## Comparative Hydrodynamic Analysis of Narrow and Pilot-Scale Bubble Columns with Internals

Möller, F.; Kipping, R.; Schleicher, E.; Löschau, M.; Hampel, U.; Schubert, M.;

Originally published:

July 2019

**Chemie Ingenieur Technik 91(2019)9, 1339-1346**

DOI: <https://doi.org/10.1002/cite.201800110>

Perma-Link to Publication Repository of HZDR:

<https://www.hzdr.de/publications/Publ-27755>

Release of the secondary publication  
on the basis of the German Copyright Law § 38 Section 4.

# Comparative Hydrodynamic Analysis of Narrow and Pilot-Scale Bubble Columns with Internals

Felix Möller<sup>1,\*</sup>, Ragna Kipping<sup>2</sup>, Eckhard Schleicher<sup>2</sup>, Martin Löschau<sup>3</sup>, Uwe Hampel<sup>1,2</sup>, Markus Schubert<sup>1</sup>

## Abstract

For a stable operation of exothermic processes in bubble column reactors, an appropriate heat control is required, e.g. through dense tube bundle heat exchangers installed in the column. However, their impact on flow morphology, phase distribution, mixing and mass transfer is scarcely reported and the derivation of reliable scaling approaches for bubble columns with internals is challenging. Thus, a narrow column (DN100) and a pilot-scale column (DN400) were equipped with tubes in two common patterns with triangular and square pitches to study local fluid dynamics. The results of both reactors are discussed with regard to their hydrodynamic similarity.

## Keywords

Bubble column scale-up, Heat exchanger internals, Hydrodynamic similarity, Ultrafast X-ray tomography, Wire-mesh sensor

## 1 Introduction

Bubble columns are widely applied in the chemical process industry due to their excellent heat and mass transfer performance at lower energy input compared to other multiphase contactors [1]. Furthermore, they have a simple design without moving parts and require low maintenance. Bubble columns are often used for hydrogenations, oxidations and bioprocesses as well as for waste-water treatment etc. Since most of the reactions in bubble columns are of exothermic nature, an appropriate heat management is required to ensure isothermal reaction conditions with high product selectivity and stable reactor operation [2,3]. Internals with tube bundles are mostly applied to efficiently remove the reaction heat. The Fischer-Tropsch synthesis is a typical example, which requires a large specific heat exchanger area of up to  $45 \text{ m}^2\text{m}^{-3}$  [4,5]. Accordingly, between 20 % and 60 % of the cross-sectional area is covered by the tubes [2,6,7]. While a coverage of approx. 5 % and below has hardly any effect [7–15], values larger than 20 % have a significant influence on the hydrodynamics. Compared to empty columns, the average gas holdup in columns with internals is increasing due to smaller and slower rising bubbles as a result of the prevailing breakup bubble formation mechanism [10,14,16–18]. Tracer experiments have shown that internals also favor larger liquid circulation cells and suppress radial spreading and dispersion [18–20]. Recent studies in a narrow column revealed that internals favor asymmetric flow patterns [16–18], while comparable analyses at pilot-scale are not yet available.

---

<sup>1</sup> Felix Möller (felix.moeller@hzdr.de), Eckhard Schleicher, Prof. Uwe Hampel, Dr. Markus Schubert, Helmholtz-Zentrum Dresden-Rossendorf, Bautzner Landstr. 400, 01328 Dresden

<sup>2</sup> Ragna Kipping, Prof. Uwe Hampel, AREVA Endowed Chair of Imaging Techniques in Energy and Process Engineering, Technische Universität Dresden, 01062 Dresden, Germany

<sup>3</sup> Martin Löschau, Teletronic Rossendorf GmbH, Bautzner Landstr. 45, 01454 Radeberg/OT Rossendorf

The hydrodynamics were intensively studied for different column dimensions and several scaling approaches were derived for empty bubble columns. Gas holdup,  $\varepsilon_g$ , and mass transfer,  $k_1a$ , are weak functions of the column diameter,  $D$ , [21], while gas and liquid dispersion coefficients,  $D_g$  and  $D_l$ , interfacial area,  $a$ , Sauter mean diameter,  $d_{32}$ , flow patterns, flow regime transition, liquid circulation velocity,  $u_{rec}$ , and center line liquid velocity,  $u_{lz}$ , as well as the large bubble holdup depend strongly on the reactor diameter [22–24]. The most relevant hydrodynamic parameters and their relation to the column diameter are summarized in Tab. 1.

**Table 1**

Typically, the derived scale-up correlations consider average parameters accessible with conventional measurement techniques. However, such average parameters do not capture possible variations in local flow structures and evolving profiles, which are decisive for the column operation [25–27]. Ignoring those local effects can lead to unexpected process behavior.

Safonuk et al. [28] and Macchi et al. [29] proposed a scaling approach based on Morton number, Eötvös number, Reynolds number, density ratio and velocity ratio, albeit basically developed for fluidized-bed reactors. However, despite identical dimensionless numbers in different reactor geometries they still observed strongly diverging flow dynamics, e.g. pressure fluctuations, which are not properly considered during scale-up. Accordingly, such different flow dynamics at different scales cause the formation of swirls, local eddies as well as asymmetries, which, for example, can lead to the formation of unexpected hotspots [30].

Shaikh et al. [21,31] also revealed that columns with the same average parameters, e.g. average gas holdup, average bubble rise velocity, etc., can vary locally. Therefore, they suggested a scale-up strategy based on the similarity of radial gas holdup profile, liquid velocity profile, average gas holdup and centerline liquid velocity regardless of the column dimensions. However, local bubble size distributions, which are also decisive for pressure gradients, the formation of holdup profiles as well as velocity gradients, were not considered [1]. Interestingly, they cross-checked the dimensionless groups approach of Safonuk et al. [28] and Macchi et al. [29], which revealed different dimensionless numbers even though average as well as local hydrodynamic properties were successfully matched.

The scale-up approaches discussed above refer to empty BCRs only. Hitherto, no reliable scaling method for bubble columns with internals is available. Thus, a first attempt is made in this study to comparatively investigate local hydrodynamic parameters of a narrow (DN100) and a pilot-scale column (DN400) equipped with two common tube patterns with triangular and square pitches using advanced imaging techniques. The results are discussed with regard to hydrodynamic similarities of both reactors.

## 2 Experimental setup

### 2.1 Column and internals design

Columns of 0.10 m are often applied for laboratory bubble column studies [22,32,33]. On the other hand, it is commonly assumed that columns with diameters larger than 0.30 m are required to obtain results applicable for industrial scales [20,34,35]. Thus, experiments were carried out in a narrow column of

0.10 m inner diameter (DN100) and a pilot-scale column of 0.39 m inner diameter (DN400) shown in Fig. 1.

### Figure 1

The clear liquid heights,  $H_c$ , were adjusted at 1.1 m and 2.6 m for narrow and pilot-scale column, respectively, corresponding to  $H_c/D \approx 11$  for the narrow and  $H_c/D \approx 7$  for the pilot-scale column, which are well above  $H_c/D \approx 5$ , where  $H_c$  has no effect on the hydrodynamics [25]. Perforated plate spargers with hole diameters of  $0.5 \times 10^{-3}$  m arranged in a triangular pitch of  $1 \times 10^{-2}$  m were used with a free area of 0.14%, which equals 55 holes for the DN100 and 861 holes for the DN400 sparger to ensure the same inlet bubble size spectra in both columns. The superficial gas velocity was adjusted with mass flow controllers (FMA2011a and FMA2013a, Omega) between  $0.01$  and  $0.20 \text{ m s}^{-1}$  (based on the free area). Results for  $0.12 \text{ m s}^{-1}$  are shown and discussed here representing the churn-turbulent flow regime, which is commonly present in industrial columns [34,36].

Internals patterns with triangular and square pitches were used with tube diameters of  $8 \times 10^{-3}$  m and  $32 \times 10^{-3}$  m for narrow and pilot-scale column, respectively. The wall area was kept free of internals to promote the heat transfer and for easier maintenance [11,37]. As design parameters for the two scaled columns, similar tube-to-pitch diameter ratio, free wall region and coverage as well as same number of tubes were used. The coverage was fixed at  $\sim 25\%$  for all internals, which is a typical value for Fischer-Tropsch reactors. The geometrical details of the internals are summarized in Tab. 1.

### Table 2

The tubes were tightly fixed in the column via 3D-printed spacers for the narrow column and via lasered stainless steel spacers for the pilot-scale column installed every 0.5 m (see Fig. 1).

## 2.2 Measurement techniques

For the narrow column, ultrafast X-ray computed tomography was used to non-invasively measure local gas holdup distribution and bubble size distribution. For the pilot-scale column, custom-made wire-mesh sensors (WMS) were used.

### Figure 2

Compared to medical and conventional process X-ray scanners, the ultrafast X-ray tomography (Fig. 2) operates without moving parts. Instead, an electron beam is rapidly swept across a circular tungsten target surrounding the column producing a moving X-ray spot. A detector ring with 432 detector elements is mounted around the column to record the intensity of the X-rays passing the column. This enables imaging frequencies of up to  $8000 \text{ frames s}^{-1}$  (note that  $1000 \text{ frames s}^{-1}$  and a total scanning time of 10 s

were chosen in this work). Furthermore, simultaneous measurements at two planes with an axial distance of about  $11 \times 10^{-3}$  m were carried out. Reconstruction algorithms (e.g. filtered back projection) to obtain images with a spatial resolution of roughly  $0.5 \times 10^{-3}$  m and post-processing steps (e.g. normalizing, referencing, thresholding) are required to extract hydrodynamic parameters. Details about the imaging technique and the post-processing can be found elsewhere [16,18,38]. The measurement height was adjusted at  $H_c/D = 5$ , which is located at well-developed flow conditions.

### Figure 3

Contrary to tomography, the WMS technique is an invasive imaging method, which basically consists of two orthogonally arranged wire planes acting as transmitter and receiver, respectively, to determine conductance or permittivity of fluids or fluid mixtures in the virtual crossing points (Fig. 3). By sequential excitation of the wires in the transmitter plane and measuring the resulting current flow at all receiver electrodes in parallel, one is able to acquire the electrical conductance within each single crossing point of the sensor with frame rates of up to  $10,000 \text{ frames s}^{-1}$ . This way, gas can be distinguished from the liquid to study the gas-liquid flow morphology. Moreover, conductivity tracers can be added to study liquid mixing [18,39]. The spatial resolution of WMS depends on the application and is usually in the range of  $3.5 \times 10^{-3}$  m for pipe flows and  $5..10 \times 10^{-3}$  m for larger bubble columns. A three-layer WMS (one transmitter layer and two receiver layers with a proper excitation scheme) was installed to optionally obtain the gas phase velocity information (not shown in this study) cross-correlating the simultaneous measured gas-liquid distributions of both planes. The WMSs consist of  $64 \times 64$  wires with a lateral spacing of  $6.125 \times 10^{-3}$  m and a plane distance of  $4 \times 10^{-3}$  m. The measurement frequency was set to  $2500 \text{ frames s}^{-1}$  and the measurement durations was 24 s. The WMS measurement position was also at  $H_c/D = 5$ .

While WMS can be easily installed in the cross-section of pipes and empty columns, special inlays (with same diameter as the tubes) were designed and manufactured to cope with the internals crossing the wire-mesh (see Fig. 2). The middle parts of the segmented inlays contain notch patterns to embed the wires from the adjacent layers. Eventually, the segments were connected with the internal tubes. The head parts of the inlays were connected with the spacer, which takes up the weight of inlays and tubes. Similar studies were carried out in a rod bundle mock up assessing a wire-mesh sensor within the tube bundle [40]. By using the referencing method, e.g. measuring the dynamic liquid gas flow as well as a liquid reference without gas, one can calculate the gas fraction within the cross-section. Having this information, bubble detection algorithms are applied in order to extract single bubbles for the calculation of a bubble size distribution. More details on WMS applications and data post-processing can be found elsewhere [18,41–44].

## 3 Results and Discussion

The hydrodynamic parameters of narrow and pilot-scale bubble columns with internals were studied for a wide range of operating conditions. In this work, cross-sectional gas holdup distributions, local bubble size distributions and flow morphologies for a superficial gas velocity of  $0.12 \text{ m s}^{-1}$  are exemplarily shown and discussed with regard to scalability between both columns in terms of hydrodynamic similarity. The gas holdup distribution is decisive for the velocity profiles [45,46]. As the liquid motion is induced by bubbles moving through the liquid, the bubble size distribution reveals insights regarding liquid circulation and liquid centerline velocity.

### 3.1 Gas holdup distribution

In Fig. 3, radial gas holdup profiles (bottom) are shown, obtained for the time-averaged cross-sectional holdup images (top). It should be noted that the respective parts covered by the inlays and internals, respectively, were masked before calculating the profiles. The values of the average holdup are incorporated within the radial profile plots.

Figure 4

Although the measurements were performed at column heights ensuring a fully developed flow, the cross-sectional images confirm that internals induce moderate flow asymmetries regardless of the column diameter (e.g. higher gas fraction at the left wall region for DN400/T32 and DN100/T8) [25]. These asymmetric flow patterns were stable over the measurement time of 10 and 24 seconds, respectively. On a longer time frame of several minutes, the cross-sectional patterns were slowly rotating, however, maintaining the characteristic asymmetries. Thus, the holdup profiles obtained from the exemplary distribution patterns are representative for the radial phase distribution.

Compared to the typical parabolic profile known from empty bubble columns [38], the internals significantly alter the gas holdup distribution regardless of the column diameter. Polynomial fluctuations evolve within the bundle, which are attributed to the parabolic holdup profile forming within every sub-channel as a result of the no-slip flow condition at the tubes walls. Close to the column wall, where no internals are placed, a parabolic distribution is encountered.

The gas preferably rises within the wall region (as shown by the higher gas fraction) resulting from the internals acting as flow resistance for the gas phase. However, this is more pronounced for the narrow column with lower hydraulic diameter of the sub-channels (factor 4), which scales with the internals diameter.

In terms of scale-up, the radial holdup profile can be used as a scaling quantity between the two diameters since both holdup curves feature a similar trend and shape as well as the average holdup values are in a similar range. It can be concluded that geometrical scaling of the internals (tube-to-pitch diameter ratio, number of tubes, coverage, free wall region) results in similar holdup characteristics and, hence, hydrodynamic similarity of the local flow structures for both columns.

### 3.2 Bubble size distribution and gas phase morphology

The imaging techniques visualize the temporal evolution of the gas structures only. Thus, the time axis requires a proper scaling applying the gas velocity data. The structures (bubbles) identified in subsequent cross-sectional images are scaled based on the average gas velocity (not shown in this study) obtained via cross-correlating both measurement planes. This way, shape and volume of individual gas bubbles can be approximated. Figs. 5 and 6 show the bubble size distributions for both columns as well as the pseudo-3D flow structures, i.e. the temporal evolution of the gas phase flow morphology.

Figure 5

A bimodal bubble size distribution is obtained for the narrow column (solid line) as known for empty BCRs operated at churn-turbulent flow conditions [47]. Here, the column wall stabilizes larger bubbles in the region without internals. At the same time, small bubbles are prevailing within the sub-channels as breakup is the dominating bubble formation mechanism. For the pilot-scale column, however, the peak for larger bubbles disappears due to the marginal column wall effect. It should be noted that the spatial resolution of the WMS is  $6.125 \times 10^{-3} \text{ m}$ , which leads to a slight underestimation of bubbles smaller than the wire spacing. However, a clearly wider distribution is obtained for the pilot-scale column with a peak at approx.  $1 \times 10^{-2} \text{ m}$ , while the first peak (representing the small bubbles) for the narrow bubble column is at  $5 \times 10^{-3} \text{ m}$ , which is due to the smaller sub-channel size. The larger bubbles, which are created for the pilot-scale column, induce an increasing centerline as well as liquid circulation velocity, which is in line with the literature (see Tab. 1), revealing a strong influence of the column diameter on the liquid motion.

The pseudo-3D plots compiled in Fig. 6 show larger bubbles in the wall region of the narrow column, whereas the bubble distribution within the cross-section of the pilot-scale column is more uniform and the wall effect is negligible.

### Figure 6

Fig. 6 further highlights that both columns with internals feature helical flow structures, which is also known from empty bubble columns [30]. However, the bubble size depends strongly on the wall effects as well as on the sub-channel size. For empty bubble columns with an inner diameter of  $D > 0.15 \text{ m}$ , wall effects are negligible [25]. The validity of such thumb rule is not yet confirmed for bubble columns with internals, where the sub-channel layout (square, triangular, circular, etc.), tube size as well as the free wall region are important parameters for the stabilizing wall effect. According to the conclusion of Wilkinson et al. [25], where the wall effect is negligible for columns larger than  $0.15 \text{ m}$ , and accounting for 25 % tube coverage, the wall effect in columns with diameters larger than  $0.2 \text{ m}$  should be negligible. However, since the sub-channels introduce additional wall area, such rule may not hold as the hydraulic sub-channel diameters should be larger than  $0.15 \text{ m}$  in order to suppress the stabilizing sub-channel wall effect. Therefore, a column diameter where wall effects are negligible might be found for columns larger than  $0.2 \text{ m}$ . However, the sub-channel wall effect will always be present.

Since the sub-channel diameter can be identified as the most crucial design parameter, similar sub-channel sizes are required to achieve comparable bubble size distributions and flow structures in columns of different scales. This, however, results in a larger occlusion area as well as higher flow friction. Hence, smaller bubbles will be formed for larger columns, which, in turn, results in decreased liquid velocity and centerline liquid velocity. Therefore, such strategy would ensure hydrodynamic similarity with regard to the liquid velocity profile.

## 4 Conclusion

In this work, a hydrodynamic analysis of narrow and pilot-scale bubble columns with internals was carried out at churn-turbulent flow conditions ( $0.12 \text{ m s}^{-1}$ ). The results were discussed with regard to hydrodynamic similarity based on local flow data, such as radial holdup distribution, bubble sizes distribution and flow structures. Local flow structures and cross-sectional holdup distribution depend strongly on the free area distribution, i.e. the area kept free of internals. The bubble size distribution in the

pilot-scale column is rather broad, while it exhibits a two bubble-class distribution in the narrow column, caused by the stabilizing wall effect and the smaller sub-channel diameter for the narrow bubble column and vice versa.

As a first outcome, the geometrical scaling quantities for such heat exchanger internals, namely pitch-to-tube diameter ratio, coverage, number of tubes and free wall region, are a proper selection to achieve hydrodynamic similarity for both columns. The results also reveal that the sub-channel size should be kept constant, too. However, this leads to higher tube coverage for large-scale reactors. This leads to an optimization problem confined by the keeping same sub-channel size and tube coverage, while maintaining the heat transfer performance, e.g. the heat transfer area. Thus, the tube diameter needs to be scaled accordingly in order to close the optimization problem as well as to achieve hydrodynamic similarity. Furthermore, the free area distribution in the reactor's cross-section can be used as a scaling quantity. By keeping it constant for different diameters, the occurring profiles and hydrodynamic properties should follow the free area distribution.

## Acknowledgments

The authors gratefully acknowledge the European Research Council (ERC StG, No. 307360) for financial support.

## Symbols used

### Symbols

$a$	[m <sup>-1</sup> ]	Interfacial area
$D$	[m]	Column diameter
$D_g$	[m <sup>2</sup> s <sup>-1</sup> ]	Gas dispersion coefficient
$D_l$	[m <sup>2</sup> s <sup>-1</sup> ]	Liquid dispersion coefficient
$d_{32}$	[m]	Sauter mean diameter
$d_e$	[m]	Equivalent diameter of a sphere
$H$	[m]	Column height
$k_1a$	[s <sup>-1</sup> ]	Volumetric mass transfer coefficient
$R$	[m]	Column radius
$r$	[-]	Radial position within the cross-section
$u_g$	[m s <sup>-1</sup> ]	Superficial and local gas velocity
$u_{l,z}$	[m s <sup>-1</sup> ]	Center line liquid velocity
$u_{rec}$	[m s <sup>-1</sup> ]	Recirculation liquid velocity

### Greek symbols

$\varepsilon_g$	[-]	Radial holdup distribution
-----------------	-----	----------------------------

### Abbreviations

WMS	Wire-mesh sensor
-----	------------------

### References



- [1] W.-D. Deckwer, A. Schumpe, *Chem. Eng. Sci.* **1993**, *48* (5), 889–911. DOI: [http://dx.doi.org/10.1016/0009-2509\(93\)80328-N](http://dx.doi.org/10.1016/0009-2509(93)80328-N).
- [2] S. Schlüter, A. Steiff, P.-M. Weinspach, *Chem. Eng. Process. Process Intensif.* **1995**, *34* (3), 157–172. DOI: [http://dx.doi.org/10.1016/0255-2701\(94\)04002-8](http://dx.doi.org/10.1016/0255-2701(94)04002-8).
- [3] P. Rollbusch, M. Bothe, M. Becker, M. Ludwig, M. Grünewald, M. Schlüter, R. Franke, *Chem. Eng. Sci.* **2015**, *126*, 660–678. DOI: <http://dx.doi.org/10.1016/j.ces.2014.11.061>.
- [4] F. Hugues, B. Szymkowiak, J. C. Viguie, J. M. Schweitzer, M. Munier, D. Chretien, E. Caprani, D. Douziech, *US Patent US7776287*, **2010**.
- [5] C. Maretto, V. Piccolo, J. C. Viguie, G. Ferschneider, *US Patent US6348510 B1*, **2002**.
- [6] S. Berg, S. Schlüter, *Chem. Ing. Tech.* **1995**, *67* (3), 289–299. DOI: 10.1002/cite.330670305.
- [7] A. A. Youssef, M. H. Al-Dahhan, M. P. Duduković, *Int. J. Chem. Reactor Eng.* **2013**, *11* (1), 169–223.
- [8] S. Berg, *Ph.D. thesis*, TU Dortmund **1993**.
- [9] K. Bernemann, *Ph.D. thesis*, TU Dortmund **1989**.
- [10] M. Hamed, *Ph.D. thesis*, Washington University St. Louis **2012**.
- [11] A. A. Youssef, *Ph.D. thesis*, Washington University St. Louis **2010**.
- [12] H.-J. Korte, *Ph.D. thesis*, TU Dortmund **1987**.
- [13] K. Bernemann, A. Steiff, P.-M. Weinspach, *Chem. Ing. Tech.* **1991**, *63* (1), 76–77. DOI: 10.1002/cite.330630120.
- [14] A. A. Youssef, M. H. Al-Dahhan, *Ind. Eng. Chem. Res.* **2009**, *48* (17), 8007–8013. DOI: 10.1021/ie900266q.
- [15] A. A. Youssef, M. E. Hamed, M. H. Al-Dahhan, M. P. Duduković, *Chem. Eng. Res. Des.* **2014**, *92* (9), 1637–1646. DOI: 10.1016/j.cherd.2013.12.011.
- [16] F. Möller, Y. M. Lau, T. Seiler, U. Hampel, M. Schubert, *Chem. Eng. Sci.* **2018**, *179*, 265–283. DOI: <https://doi.org/10.1016/j.ces.2018.01.008>.
- [17] Y. M. Lau, F. Möller, U. Hampel, M. Schubert, *Int. J. Multiphase Flow.* **2018**. DOI: <https://doi.org/10.1016/j.ijmultiphaseflow.2018.02.009>.
- [18] F. Möller, A. MacIsaac, Y. M. Lau, E. Schleicher, U. Hampel, M. Schubert, *Chem. Eng. Res. Des.* **2018**.
- [19] K. J. H. George, *Master's thesis*, The University Of Western Ontario **2015**.
- [20] A. Forret, J.-M. Schweitzer, T. Gauthier, R. Krishna, D. Schweich, *Can. J. Chem. Eng.* **2003**, *81* (3-4), 360–366. DOI: 10.1002/cjce.5450810304.
- [21] A. Shaikh, M. Al-Dahhan, *Ind. Eng. Chem. Res.* **2013**, *52* (24), 8091–8108. DOI: 10.1021/ie302080m.
- [22] W. D. Deckwer, *Bubble Column Reactors*, John Wiley & Sons Inc **1992**.
- [23] M. H. I. Baird, R. G. Rice, *Chem. Eng. J.* **1975**, *9* (2), 171–174. DOI: [http://dx.doi.org/10.1016/0300-9467\(75\)80010-4](http://dx.doi.org/10.1016/0300-9467(75)80010-4).
- [24] S. Degaleesan, M. P. Dudukovic, B. A. Toseland, B. L. Bhatt, *Ind. Eng. Chem. Res.* **1997**, *36* (11), 4670–4680. DOI: 10.1021/ie970200s.
- [25] P. M. Wilkinson, A. P. Spek, L. L. van Dierendonck, *AIChE J.* **1992**, *38* (4), 544–554. DOI: 10.1002/aic.690380408.
- [26] J. R. Inga, B. I. Morsi, *Can. J. Chem. Eng.* **1997**, *75* (5), 872–881. DOI: 10.1002/cjce.5450750507.
- [27] L.-S. Fan, G. Q. Yang, D. J. Lee, K. Tsuchiya, X. Luo, *Chem. Eng. Sci.* **1999**, *54* (21), 4681–4709. DOI: [https://doi.org/10.1016/S0009-2509\(99\)00348-6](https://doi.org/10.1016/S0009-2509(99)00348-6).
- [28] M. Safoniuk, J. R. Grace, L. Hackman, C. A. McKnight, *Chem. Eng. Sci.* **1999**, *54* (21), 4961–4966. DOI: [https://doi.org/10.1016/S0009-2509\(99\)00218-3](https://doi.org/10.1016/S0009-2509(99)00218-3).
- [29] A. Macchi, H. Bi, J. R. Grace, C. A. McKnight, L. Hackman, *Chem. Eng. Sci.* **2001**, *56* (21), 6039–6045. DOI: [https://doi.org/10.1016/S0009-2509\(01\)00207-X](https://doi.org/10.1016/S0009-2509(01)00207-X).
- [30] R. C. Chen, J. Reese, L. S. Fan, *AIChE J.* **1994**, *40* (7), 1093–1104. DOI: 10.1002/aic.690400702.
- [31] A. Shaikh, M. Al-Dahhan, *Can. J. Chem. Eng.* **2010**, *88* (4), 503–517. DOI: 10.1002/cjce.20357.
- [32] Y. Ohki, H. Inoue, *Chem. Eng. Sci.* **1970**, *25* (1), 1–16. DOI: [http://dx.doi.org/10.1016/0009-2509\(70\)85016-3](http://dx.doi.org/10.1016/0009-2509(70)85016-3).
- [33] R. Badura, W.-D. Deckwer, H.-J. Warnecke, H. Langemann, *Chem. Ing. Tech.* **1974**, *46* (9), 399–399. DOI: 10.1002/cite.330460909.
- [34] Y. T. Shah, B. G. Kelkar, S. P. Godbole, W.-D. Deckwer, *AIChE J.* **1982**, *28* (3), 353–379. DOI: 10.1002/aic.690280302.
- [35] Y. T. Shah, C. A. Ratway, H. G. McIlvried, *Trans. Inst. Chem. Eng.* **1978**, *56* (2), 107–112.
- [36] S. Nedeltchev, F. Möller, M. Schubert, in *Proceedings (MMPE)* **2017**.
- [37] H. Li, A. Prakash, *Can. J. Chem. Eng.* **2001**, *79* (5), 717–725. DOI: 10.1002/cjce.5450790503.

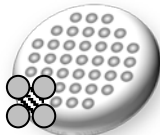
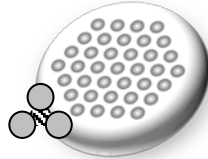
- [38] F. Möller, T. Seiler, Y. M. Lau, M. Weber, M. Weber, U. Hampel, M. Schubert, *Chem. Eng. J.* **2017**, *316*, 857–871. DOI: <http://dx.doi.org/10.1016/j.cej.2017.01.114>.
- [39] R. Kipping, H. Kryk, E. Schleicher, M. Gustke, U. Hampel, *Chem. Eng. Technol.* **2017**, *40* (8), 1425–1433. DOI: 10.1002/ceat.201700005.
- [40] A. T. Ylönen, *thesis*, ETH Zürich **2013**.
- [41] R. Kipping, R. Brito, E. Scheicher, U. Hampel, *Int. J. Multiphase Flow.* **2016**, *85*, 86–95. DOI: <http://dx.doi.org/10.1016/j.ijmultiphaseflow.2016.05.017>.
- [42] H.-M. Prasser, A. Böttger, J. Zschau, *Flow Meas. Instrum.* **1998**, *9* (2), 111–119. DOI: [http://dx.doi.org/10.1016/S0955-5986\(98\)00015-6](http://dx.doi.org/10.1016/S0955-5986(98)00015-6).
- [43] R. Kipping, H. Kryk, E. Schleicher, M. Gustke, U. Hampel, *Chem. Eng. Technol.* **2017**, *40* (8), 1425–1433. DOI: 10.1002/ceat.201700005.
- [44] H. Pietruske, H.-M. Prasser, *Flow Meas. Instrum.* **2007**, *18* (2), 87–94. DOI: <https://doi.org/10.1016/j.flowmeasinst.2007.01.004>.
- [45] H. Luo, H. F. Svendsen, *Can. J. Chem. Eng.* **1991**, *69* (6), 1389–1394. DOI: 10.1002/cjce.5450690622.
- [46] J.-M. Schweitzer, J. Bayle, T. Gauthier, *Chem. Eng. Sci.* **2001**, *56* (3), 1103–1110. DOI: [http://dx.doi.org/10.1016/S0009-2509\(00\)00327-4](http://dx.doi.org/10.1016/S0009-2509(00)00327-4).
- [47] P. Gupta, B. Ong, M. H. Al-Dahhan, M. P. Dudukovic, B. A. Toseland, *Catal. Today.* **2001**, *64* (3-4), 253–269. DOI: [http://dx.doi.org/10.1016/S0920-5861\(00\)00529-0](http://dx.doi.org/10.1016/S0920-5861(00)00529-0).
- [48] K. Akita, F. Yoshida, *Ind. Eng. Chem. Process Des. Dev.* **1974**, *13* (1), 84–91. DOI: 10.1021/i260049a016.
- [49] K. Akita, F. Yoshida, *Ind. Eng. Chem. Process Des. Dev.* **1973**, *12* (1), 76–80. DOI: 10.1021/i260045a015.
- [50] K.-H. Mangartz, T. Pilhofer, *Verfahrenstechnik (Mainz)*. **1980**, *14* (1), 40–44.
- [51] J. B. Joshi, *Chem. Eng. Res. Des.* **1980**, (58A), 155–165.

## Tables with headings

Table 1: Influence of the column diameter on hydrodynamic parameters.

Parameter	Influence of column diameter	Author
$\varepsilon_g$	$0.07u_g^{0.474-0.000626D}$	[24]
$a$	$\sim D^{0.3}$	[48]
$k_1a$	$\sim D^{0.17}$	[49]
$D_g$	$\sim D^{1.5}$	[50]
$D_z$	$\sim D^{1.4}$	[33]
$u_{lz}$	$\sim D^{0.33}$	[51]
$u_{rec}$	$\sim D^{0.4}$	[24]
$d_{32}$	$\sim D^{0.3}$	[48]

Table 2: Geometric specifications of the internals for narrow and pilot-scale columns.

Pattern				
	Square 8	Square 32	Triangular 8	Triangular 32
Tube diameter ( $\times 10^{-3}$ m)	8	32	8	32
Tube-to-pitch diameter ratio (-)	1.38	1.34	1.44	1.43
Coverage (%)	24	24	24	24
Number of tubes (-)	37	37	37	37
Hydraulic sub-channel dia. ( $\times 10^{-3}$ m)	7.62	28.76	5.57	22.19
Sub-channel area ( $\times 10^{-6}$ m <sup>2</sup> )	70.73	1036.16	32.13	510.15

## Figure legends

Figure 1: Schematic drawing of the experimental setup with CAD drawings of the bubble columns and the internals installation.

Figure 2: DN100 column setup mounted within the ultrafast X-ray scanner facility.

Figure 3: Wire-mesh sensor with inlays for the tube alignment and spacers for the tube fixation.

Figure 4: Radial gas holdup profiles for a) triangular and b) square configurations with corresponding cross-sectional holdup distributions (the vertical dashed line represents the end of the tube bundle).

Figure 5: Bubble size distributions for a) square and b) triangular configurations.

**Figure 6: Pseudo-3D plots (vertical axis represents 1 s measurement time, columns are not to scale) of the gas phase morphology (note that bubbles larger than  $1 \times 10^{-3}$  m diameter are highlighted in a darker gray for the DN100 columns and arrows indicate the helical flow.**

### **Short text for table of contents section (TOC)**

Heat exchanger internals are utilized to remove reaction heat from highly exothermic processes in bubble columns. The internals' coverage significantly alters the hydrodynamics. This work compares gas holdup, bubble size distribution and flow morphology in columns at different scales and proposes a first scale-up approach with regard to hydrodynamic similarities.